Available online at www.elixirpublishers.com (Elixir International Journal)

Materials Science

Elixir Materials Science 95 (2016) 41945-41951

ISSN: 2229-712X

# Synthesis, Characterization of Nickel Oxide Nanoparticles and Effect of Solution Temperature

R. Shanaj Begum and R. John Xavier*

Department of Physics, Periyar EVR College(Autonomous), Tiruchirappalli – 620 023, India.

**ARTICLE INFO**

**Article history:**

Received: 21 May 2016;

Received in revised form:

22 June 2016;

Accepted: 27 June 2016;

**Keywords**

Nickel oxide,

Cyclic voltammetry,

Specific surface area,

Capacitive behavior.

**ABSTRACT**

Nickel oxide nanoparticles were synthesized by co-precipitation method at different solution temperatures 37°C,50° C and 70°C and calcined at 700°C.The crystalline structure of NiO NPs were studied by X-ray diffractometer ( XRD).The results confirmed the cubic structure of Nickel oxide nanoparticles and the solution temperature has no effect on crystal structure .The optical properties of the NiO samples were characterized by FT-IR,UV-VIS and PL and the morphology by scanning electron microscopy. Cyclic voltammetry characterization was carried out to study the qualitative information about the potentials at which electrochemical reactions occur.



## 1.Introduction

Transition metal oxide nanoparticles have attracted much attention due to their wide spread applications. Among them, Nickel oxide has been the focus of recent attention due to its superior properties. Because of the quantum size and surface effects, NiO nanoparticles exhibit thermal, mechanical, electronic, catalytic, optical and magnetic properties that are significantly different from bulk-sized NiO particles [1,2].

NiO nanoparticles are utilized in several applications such as in the manufacture of cell electrodes [3,4], gas sensors [5], magnetic materials [6], anti ferromagnetic layers [7], electrochemical capacitors/super capacitors [8], photovoltaic devices [9], smart windows [10], electro chromic films [11], battery cathodes [12], active optical fiber [13] and catalysis [14].

Several techniques are used to synthesis NiO nanoparticles like thermal decomposition [15], sol-gel [16], spray-pyrolysis.In this article, well crystalline NiO nanoparticles were synthesized at different solution temperatures by a simple process called co-precipitation method which is effective and low cost since the starting materials are few and inexpensive.

## 2. Experimental

### 2.1 Synthesis of Nickel Oxide nanoparticles

Nickel (II) Chloride (2.6 g ) (Aldrich, 98%) was dissolved in 100 ml of de-ionized water and 6.4 g of Sodium hydroxide (NaOH) pellets were added to100 ml of de-ionized water in separate beaker. The $NiCl_2$ solution was stirred by a magnetic stirrer for 2 hours. The NaOH solution was added to the $NiCl_2$ solution drop by drop under constant stirring. The resultant light green solution was kept at room temperature and stirred for 6 hours and then refluxed for 24 hours. The greenish precipitate formed was washed with double distilled water and ethanol to remove impurity. The sample was dried at 90°C in air to remove moisture contents. The dried sample was heated at 700 °C for 5 hours. The same procedure was repeated by varying the solution temperature as 50°C, 70°C. According to Chen and Zhou, the solution temperature needs to stay below 75°C in order to prepare ultrafine nanoparticles [17].

The precursor Nickel hydroxide decomposes into Nickel Oxide on calcinations as follows

$$NiCl_2 + 2NaOH \xrightarrow{RT} Ni(OH)_2 + 2NaCl \quad (1)$$

$$Ni(OH)_2 \xrightarrow{\text{calcinations}} NiO + H_2O \quad (2)$$

### 2.2 Characterization of synthesized NiO nanoparticles.

The samples were analyzed by Powder X-Ray Diffraction (XRD) using X' Pert PRO Diffractometer with Cu $K_\alpha$ radiation of wave length 0.15406 nm in $2\theta$ range of 10°-80° operated at 40kV and 30mA. Differential Thermal Analysis (DTA), Thermo gravimetric Analysis (TGA- 4000 Perkin Elmer) ,Differential scanning calorimetry (Instrument model DSC 6000-Pyris 6) ,Fourier Transform Infrared (FT-IR) spectroscopy analysis, UV-Vis spectroscopy analysis, (Instrument model Lamda 35) and Photoluminescence spectroscopy analysis (model-LS45) were used to analyze the thermal property and optical property of the samples prepared at different solution temperatures. Morphology of NiO NPs was studied by Scanning electron microscopy (SEM). Cyclic Voltammetry experiment was performed using three electrode cell utilizing computer controlled potentiostat (Princeton, Applied Research -Versa STAT MC –AMETEK).

### 2.3 Electrochemical Characterization

Cyclic Voltammetry analysis was done using a three electrode electrochemical cell consisting of a glassy carbon electrode, saturated calomel electrode (SCE), platinum electrode as the working electrode, the reference electrode and counter electrode respectively. The Nickel Oxide NPs were added to water which acts as solvent. Ethyl Tri methyl Ammonium Bromide which acts as electrolyte was added to the test solution to ensure sufficient conductivity. The potential is swept between-1.4 V and 1.8V at a scan rate of 20 $mVs^{-1}$. The current flowing through working electrode is recorded as a function of the varying potential.

Tele: +91 431 2780286

E-mail address: rj_xavier@yahoo.com

## 3. Results and Discussion

### 3.1Structure characterization of Nickel Oxide nanoparticles

X-ray diffraction patterns of the samples R1, R2 and R3 prepared at different solution temperatures 37°C, 50° C and 70°C respectively are shown in Fig.1. It is obvious from the figure, that the all samples had same diffraction peaks and are indexed as (111), (200), (220), (311) and(222) that correspond to face centered cubic structure of NiO nano particles which are in consistent with the standard data(JCPDS –file:78-0429 , Fm-3m space group). According to the peaks indexed ,it is evident that the increase in the solution temperature has not affected the crystal structure but it affects the morphology and size of the particles. The sharpness and the intensity of the peaks indicate the well crystalline nature of the particles. The absence of any other peak illustrates the purity of the samples.

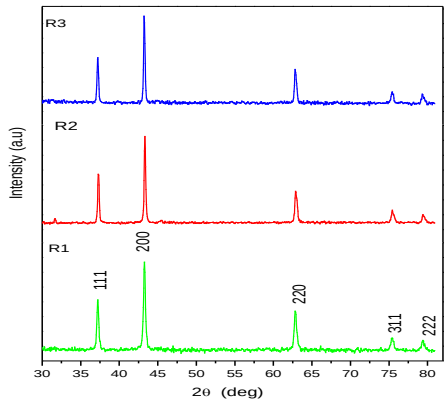


**Fig 1. XRD Patterns of the Nickel Oxide Nanoparticles at different solution temperatures.**

Crystallite size 'D' was calculated by applying the Debye-Scherer formula [18]

$$D = k\lambda / \beta\cos\theta \quad (3)$$

Where k=0.9, λ is the wavelength of Cu $k_\alpha$ radiations (1.5406 A°), β is the full width at half maximum intensity in radians,θ is the Bragg's angle. The average particle size of the NiO nanoparticles was calculated. (Table.1). It is apparent that the crystallite size increases with increasing solution temperature from 37°C to 70°C. The reason behind this may be explained as the increase in solution temperature enhanced the nucleation rate which in turn increases the crystallite size [19]. The lattice parameters calculated from XRD data deviates from its standard lattice parameter 4.177A° [20] .This may be due to strain induced in line broadening. This will mean that the size of the crystallite obtained by using Debye-Scherer formula will be slightly less than that of the actual size of the crystallite.

If both size and strain simultaneously contribute towards line broadening, the actual size of the crystallite and strain can be determined from Williamson-Hall equation [21-23] is given by

$$\beta\cos\theta = k\lambda/D + 4\varepsilon\sin\theta \quad (4)$$

Where k=0.9, ε is the strain, D represents the size of the crystallite. By plotting βcosθ along y-axis and 4Sinθ along x-axis a linear fit is got for the data and from it crystallite size and micro strain are extracted from y-intercept and slope respectively (Fig.2).The size of the crystallites of all the three samples are found and listed in table.1. It is revealed that the crystallite size estimated from Scherer formula is found to be small due to peak broadening caused by micro strain and dislocations compared to the crystallite size obtained by W.H analysis.

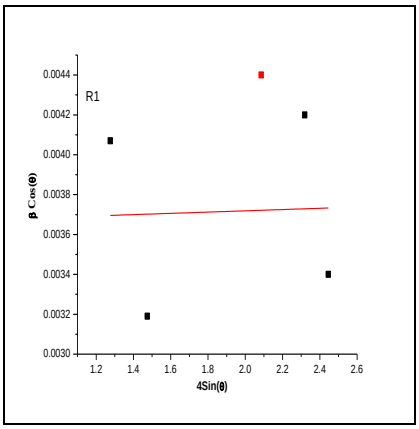


**Fig 2a. Williamson-Hall Plot for sample R1 at 37 °C.**

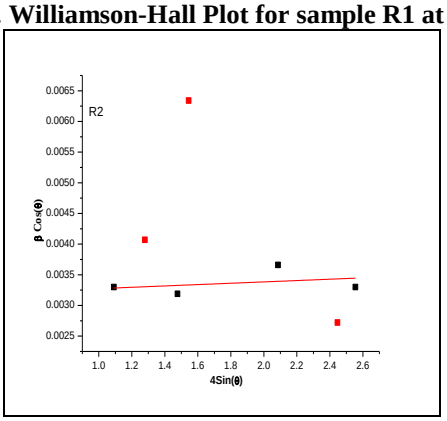


**Fig 2b. Williamson-Hall Plot for sample R2 at 50°C.**

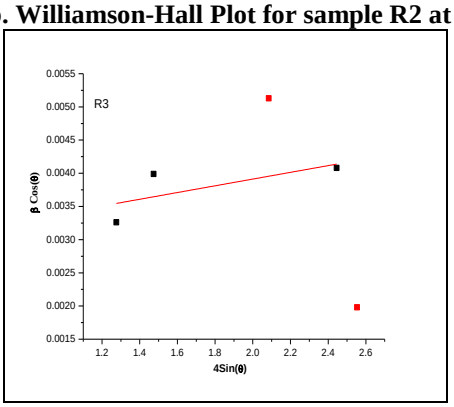


**Fig 2c . Williamson-Hall Plot for sample R3 at 70 °C.**

The micro strain ($\varepsilon$) induced in the samples due to imperfection and distortion is evaluated using the formula

$$\varepsilon = \frac{\beta}{4\tan\theta} \quad (5)$$

Where β is the FWHM intensity and θ is the peak position .The increase of solution temperature has an inverse effect on micro strain (Table.1).

**Table1.Crystallites size and XRD parameters of NiO nanoparticles at different solution temperatures.**

| Samples | Crystallite(mm) Scherer's formula | size (D) W-H plot | Micro strain *$10^{-3}$ | Dislocation density (δ) (*$10^{14}$) Lines/$m^2$ | Lattice Parameter (A°) (a) | Unit cell volume(A°)$^3$ |
|---|---|---|---|---|---|---|
| R1 | 39 | 40 | 2.43 | 6.57 | 4.200 | 74.10 |
| R2 | 41 | 44 | 2.38 | 5.95 | 4.185 | 73.30 |
| R3 | 42 | 48 | 2.04 | 5.67 | 4.184 | 7324 |

As the solution temperature increases, the decrease of the FWHM of the diffraction peaks results in the decrease of the slope indicating that the strain in the NiO lattice diminishes gradually. This decrease may be due to the fact that with the growing crystallite sizes, mobility of the ions on the surface causes reduction of imperfections like vacancies and interstitials in the crystallites [24]. The unit cell volume expands due to size reduction which is due to reduced electro static forces caused by surface dipoles. [25-27].

The dislocations and imperfections are important in growth mechanism. The dislocation density (δ) which is a measure of amount of defects can also be determined using the formula

$$\delta = 1/D^2 \quad (6)$$

Where, D is the grain size in nm. The dislocation density was evaluated for all the three samples and listed in Table 1. It is observed that the dislocation density (δ) decreases while the crystallite size increases [28]. It is due to the fact that decrease in lattice imperfections caused by increase in solution temperature leads to better crystallinity with the increased crystallite size.

Specific surface area (SSA) is a material property which is used to determine the type and properties of a material which is defined as Surface Area (SA) per mass. It can be calculated using the following relation [29] and the evaluated values are listed in Table 2.

$$SSA = (SA_{part}) / (V_{part} * density) \quad (7)$$

Where, $SA_{part}$ is surface area, $V_{part}$ is particle volume, $D_p$ is particle size, ρ is the density of NiO (6.67g/cm$^3$) [30]. From Table.2, it is evident that as the size of the particle increases, the ratio of the surface area to volume ratio decreases. If this ratio becomes significantly large, a large portion of the atoms resides on the surface where solution/interaction between NiO based devices occurs mainly [31]. And also this ratio plays an important role in changing the properties compared to bulk material [32].

**Table 2. Specific surface area of NiO nanoparticles at different solution temperatures.**

| Samples | D(nm) | Surface Area (nm) | Volume (nm)$^3$ | SSA ($m^2g^1$) | SA/ volume |
|---|---|---|---|---|---|
| R1 | 39 | 4775 | 31043 | 23.07 | 0.154 |
| R2 | 41 | 5278 | 36068 | 21.94 | 0.146 |
| R3 | 42 | 5538 | 38772 | 21.42 | 0.143 |

### 3.2 Thermal analysis

#### 3.2.1 TGA/DTA Characterization

Thermo gravimetric and the differential thermo gravimetric (TGA/DTA) analysis of the samples R1 and R3 prepared at solution temperatures 37°C and 70°C respectively, calcined at 700 °C was carried out under Nitrogen atmosphere at a heating rate of 10 °C/min in the temperature range of 35°C - 750°C to investigate the thermal behavior of the samples. TheTGA curve indicates the weight loss of 0.56% for the sample R1 (Fig.3a) and 3.45 % for the sample R3 (Fig.3b ) which are accompanied by the endothermic peaks observed at 89.61°C and 86.14°C for the samples R1and R3 in the DTG curve which are due to thermal desorption of water from the surface of the nano particles [33]. While comparing the weight losses of the samples R1 and R3, the weight loss of the sample R1 is less than that of the sample R3 which is due to the fact that the surface of the Nickel Oxide nanoparticles prepared at 37°C (sample R1) is small compared to sample R3 prepared at 70 °C (Table.2).

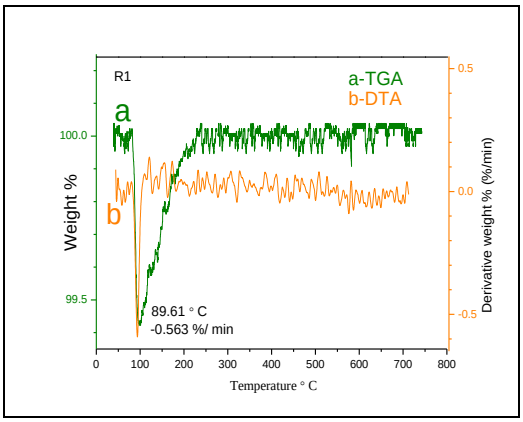


**Fig 3a. TGA–DTG plot for R1 at 37 ºC.**

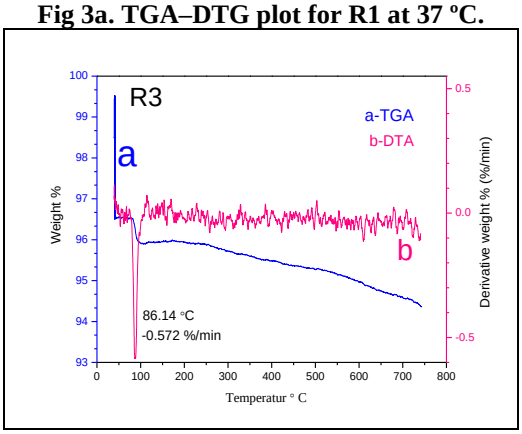


**Fig 3b . TGA–DTG plot for R3 at 70 ºC.**

#### 3.2.2 DSC Characterization

DSC analysis was also performed from 0 ° C to 445°C at 10 °C / min for the samples R1 and R3 (fig.4). The heating curves indicates two strong endothermic peaks at 92.5°C and 89.1°C for the samples R1 and R3 respectively, correspond to removal of water which is in good agreement with DTA result.

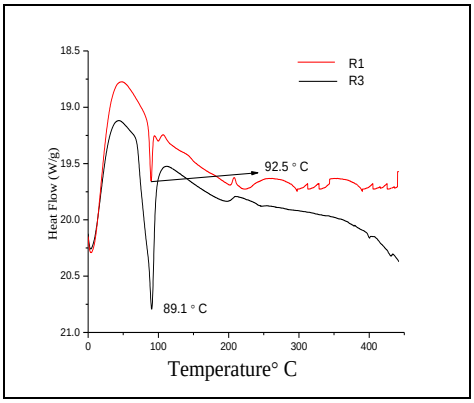


**Fig 4. DSC analysis of the samples R1 prepared at 37 ºC and R3 prepared at 70 ºC.**

### 3.3 Fourier Transform Infra Red (FT-IR) Spectroscopic Analysis

Fig.5 shows the FT-IR spectra of the samples R1, R2 and R3 prepared at different solution temperatures 37°C, 50° C and 70°C respectively. A broad absorption band at 3412 cm$^{-1}$ is the characteristic of O–H stretching bond. The band at 1597 cm$^{-1}$ is attributed to H-O-H bending vibration because of absorption of water molecule from air as the sample is synthesized in air. The absorption bands at 1393 cm$^{-1}$ and 1119 cm$^{-1}$ indicate the existence of carbonates. The band at 722 cm$^{-1}$ is assigned to Ni–O–H vibration. The band at 492 cm$^{-1}$ is associated to Ni–O vibration mode [34] which confirms the formation of Nickel Oxide nanoparticles.

It is clear from the spectra that when the solution temperatures is increased from 37°C, to 50° C and 70°C, the same functional groups are appeared with a slight change in the intensity of the bands. It is important to note that strong band exist at 494 $cm^{-1}$, 493 $cm^{-1}$ for samples R2 and R3 confirms the formation of NiO nanoparticles .Hence it is apparent that there is no change in the crystal structure of Nickel Oxide nanoparticles when the solution temperature is varied.

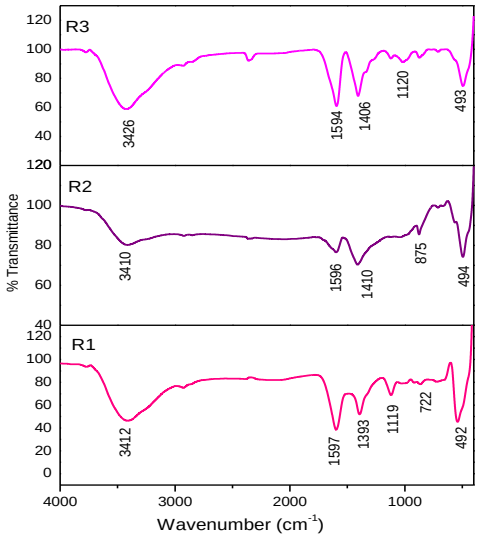


**Fig 5. FT-IR Spectra of the samples R1, R2 and R3 at different solution temperatures.**

### 3.4 UV-VIS Analysis

The formation of Nickel Oxide nanoparticles is confirmed by the appearance of Surface Plasmon absorption maxima in UV-VIS spectra of the samples R1, R2 and R3 prepared at different solution temperatures 37°C, 50° C and 70°C respectively. The peak absorption wavelengths show blue shift in their spectra (Fig.6 and the insets show corresponding absorption spectra) because of increase in the crystallite size with increase in solution temperature **(**Table.3). From the observed UV-VIS spectrum, the optical band gap is calculated using the following relational expression proposed by Tauc, Davis and Mott.

$$(Ah\nu)^n = k(h\nu - E_g) \quad (8)$$

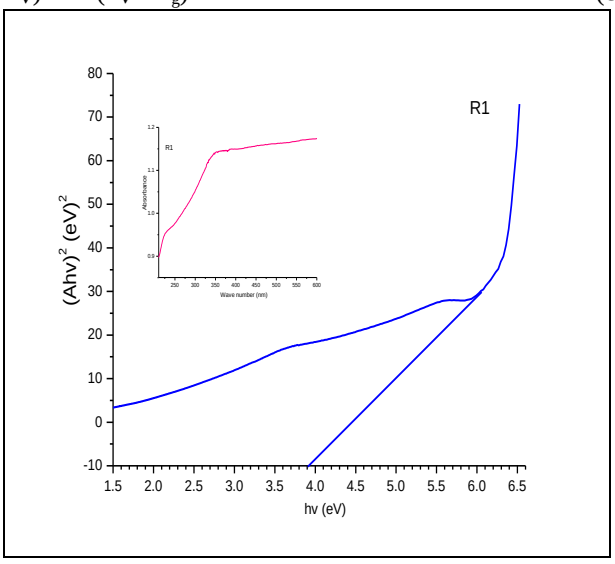


**Fig 6a. TAUC's Plot of the sample R1 and insets corresponding absorption spectra.**

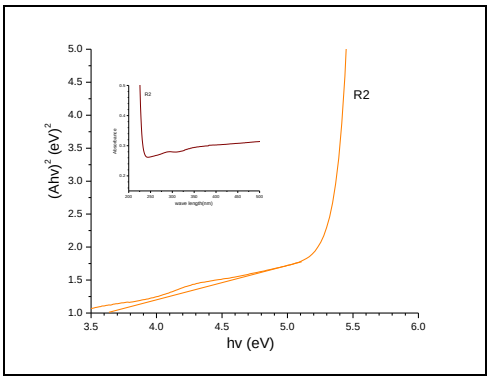


**Fig 6b. TAUC's Plot of the sample R2 and insets corresponding absorption spectra.**

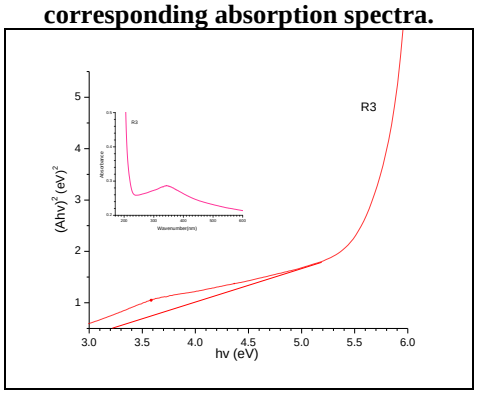


**Fig 6c.TAUC's Plot of the samples R3 and insets corresponding absorption spectra.**

Where A: the absorbance, h: Plank's constant, ν: frequency of vibration, k: material constant, $E_g$: energy gap. The value of exponent n depends on the type of transition: n = 2 for direct band gap and n= ½ for indirect band gap. The graph of $(Ah\nu)^2$ as a function of hν is plotted for direct allowed transition. The direct band gap values of Nickel Oxide nanoparticles at different solution temperatures are determined by extrapolating linear portion of the curve to energy axis and listed in Table. 3. It is apparent that the increase in both solution temperature and crystallite size leads to decrease in energy band gap which is an evidence of quantum confinement effect [35].

**Table 3.Optical parameters of NiO NPs at different solution temperatures.**

| Samples | Peak absorption Wave length ( $\lambda_{max}$) (nm) | Energy gap (eV) | Transmittance % |
|---|---|---|---|
| R1 | 325 | 3.90 | 13 |
| R2 | 337 | 3.65 | 33 |
| R3 | 342 | 3.25 | 55 |

Fig.7 shows UV-Visible transmittance spectra of the samples R1, R2 and R3. It is evident from Table.3 that the optical transmittance of the NiO nanoparticles increases as solution temperature increases.

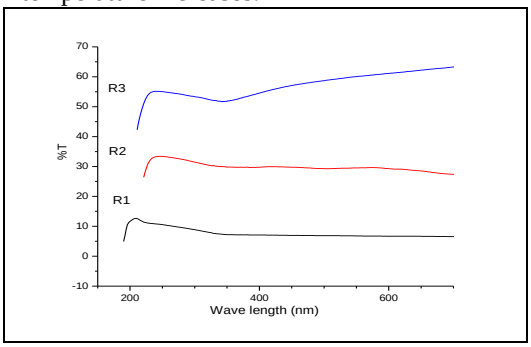


**Fig 7. Transmittance spectra of the samples R1, R2 and R3.**

### 3.5 Photoluminescence analysis

The room temperature Photoluminescence spectra of Nickel Oxide nanoparticles prepared at different solution temperatures is shown Fig.8 The sample R1 excited by 280 nm exhibits main emission peak at 303 nm (Fig.8a). The samples R2 ,R3 excited by 320 nm exhibit the main peaks at 332 nm, 364 nm and weak peaks at 338 nm ,357 nm respectively (Fig.8b, Fig.8c). The origin of main peaks and the shoulder peaks are attributed to the electronic transitions of $3d^8$ electrons of $Ni^{2+}$ ions [36, 37]. The optical absorption study reveals that there are several transitions at energies below band gap in Nickel Oxide [38]. The broad peaks in PL spectra of the samples are due to radiative recombination between electrons in the conduction band and holes in the valence band. As it is evident from Table.4 the emission peaks are shifted to lower PL energy as the particle size increases from 39nm - 42nm. This is due to the fact that oxygen vacancy is more in smaller size particles which makes absorption more hence it causes stronger PL signal. Hence the size of crystallite and the solution temperature are the main factors in the variation of PL intensity. It is concluded that, the PL intensity decreases with increase in both solution temperature and particle size [39]. In all the samples R1, R2 and R3 weak visible emissions are observed at 426 nm, 402 nm, 409 nm respectively which are due to defects-related deep level emissions like oxygen vacancies and Ni interstitials.

**Table 4. PL Energy of NiO NPs at different solution temperatures.**

| Samples | Emission Peaks (nm) | PL Intensity (a.u) | PL Energy (eV) |
|---|---|---|---|
| R1 | 303 | 41.48 | 4.09 |
| R2 | 332 | 16.73 | 3.73 |
| R3 | 364 | 12.94 | 3.41 |

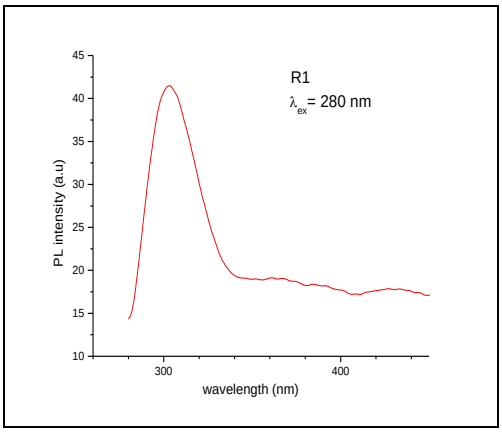


**Fig 8a. PL spectra of the sample R3 at 70 ºC.**

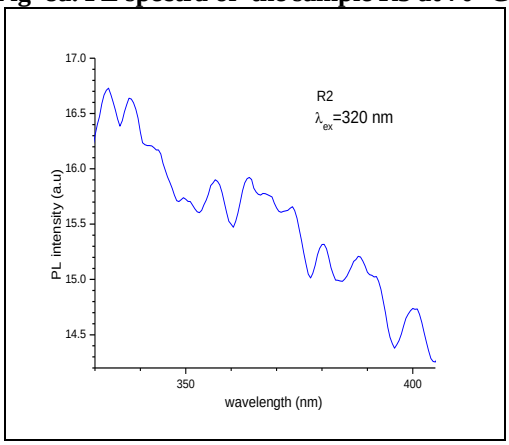


**Fig 8b. PL spectra of the sample R2 at 50 ºC.**

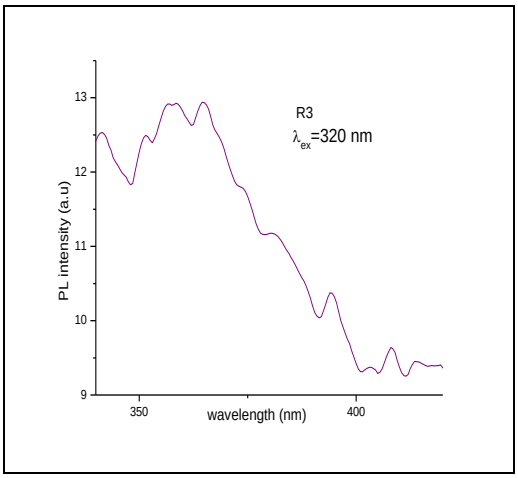


**Fig 8c. PL spectra of the sample R3 at 70 ºC.**

### 3.6 Morphology of the NiO nanoparticles

Scanning electron microscopy was used to analyze the morphology of NiO nanoparticles prepared at different solution temperatures. The SEM images (Fig 9) clearly show an agglomeration of the nanoparticles in all the samples and snowflakes like morphology at low temperature [40, 41]. As the solution temperature increases, the particles accumulate into sharp walls. It is evident that sample R3 prepared at higher temperature 70°C exhibited more defined shapes compared to the sample R1, R2 prepared at 37°C and 50°C respectively, which indicate that shape and size of the nanoparticles are influenced by the solution temperatures.

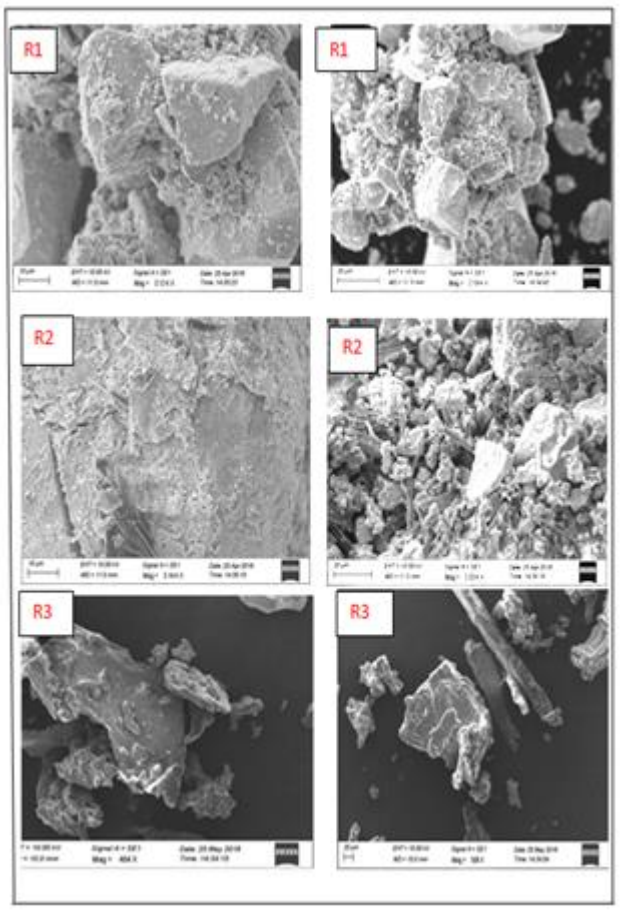


**Fig 9. SEM images of the samples R1, R2 and R3 at different magnifications.**

### 3.7 Electrochemical characterization

Fig.10 compares the cyclic voltammograms of the samples R1, R2 and R3 prepared at different solution temperatures 37°C, 50° C and 70°C respectively in the potential range of -1.4

V to 1.8V at a sweep rate of 20 $mVs^{-1}$. It is apparent that there is a pair of strong redox peaks which indicate that capacitance characteristics are controlled by Faradic reactions [42]. The redox peaks occur in all the three samples due to $Ni^{2+}$ to $Ni^{3+}$ transition at the surface of NiO NPs according to the following equation [43,44].

$$NiO + OH^- \longleftrightarrow NiOOH + e^- \quad (9)$$

The formation of NiOOH layer on the surface initiates the electro catalytic activity of NiO NPs. [45, 46]. The results indicate that sample R1 prepared at 37°C exhibits highest peak current but the sample R3 prepared at 70°C exhibits minimum peak current. The increase in current indicates that reaction activity of NiO increases with the increase in specific surface area and surface area to volume ratio (Table.2).

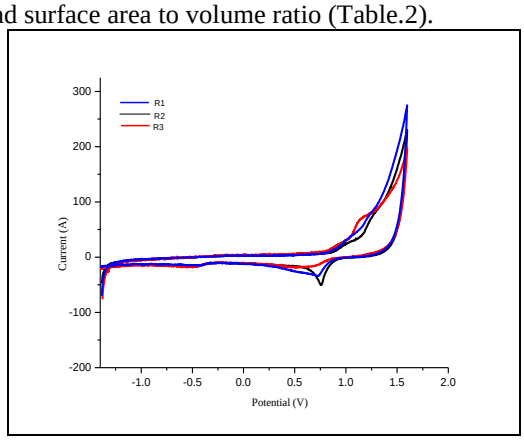


**Fig 10. Cyclic voltammograms of the samples R1, R2 and R3 at different solution temperatures.**

Since the increase in crystallite size of the sample R3 due to high solution temperature leads to decrease in both specific surface area and surface activity which leads to less capacitive behavior [47, 48]. Hence Specific surface area and surface reactivity are the main factors in determining the capacitive behavior and can be illustrated from XRD patterns of nickel oxides Fig (1), which shows a large increase in grain size at increasing solution temperature. It is concluded that sample R1 with high specific surface area have high charge-storage capability .

Specific capacitance of the samples are calculated by the formula

$$C = \int_{E1}^{E2} i(E)\, dE / 2 (E_2 - E_1)\, m\, v \quad (10)$$

where $\int_{E1}^{E2} i(E)\, dE$ is the total voltammetric charges obtained by integration of positive and negative sweep in cyclic voltammogram , ($E_2 - E_1$) is the potential window width,'m' mas of the sample and v is the scan rate. Since the anodic voltammetric charges and cathodic voltammetric charges are not same in the CV curves ,integral area of CV curve/scan rate represent the sum of anodic and cathodic voltammetric charges [49,50]. The electrochemical measurements show that samples R1, R2 and R3 prepared at different solution temperatures exhibit specific capacitance of 861 $Fg^{-1}$, 837 $Fg^{-1}$ and 836 $Fg^{-1}$ respectively. Obviously NiO nanoparticles prepared at 37°C exhibit the maximum specific capacitance. It is apparent that there is a decline of specific capacitance with the increase of solution temperature.

The position of the peaks on the potential axis ($E_p$) is related to the formal potential of the redox process. The formal potential for a reversible couple is centered between anodic peak potential ($E_{pa}$) and cathodic peak potential ($E_{pc}$) [51]

$$E^0 = (E_{pa} + E_{pc})/2 \quad (11)$$

The separation between the peak potentials $\Delta E_p$ is evaluated using the relation

$$\Delta E_p = E_{pa} - E_{pc}. \quad (12)$$

The $\Delta E_p$ for the samples R1 , R2 and R3 is 0.89V, 0.84V, and 0.82 V respectively. A fast one-electron transfer would exhibit a $\Delta Ep$ = 0.059 V at 298 K [52]. The discrepancy from this ideal value is attributed to slow electron transfers and solution resistance.

## 4. Conclusion

Nickel Oxide nanoparticles were prepared by co-precipitation method at various solution temperatures. XRD studies confirmed the FCC structure of the NiO nanoparticles and the average particle size increases from 39 nm to 42 nm with increasing the solution temperatures. The optical properties of the samples were elucidated by FTIR, UV-VIS, PL Spectroscopy. The morphologies of the samples were observed by SEM analysis. Cyclic voltammetry analysis of the samples revealed that particles with smaller size have high electrochemical reaction activity due to high specific surface area and an excellent capacitance behavior which is very important for electrode materials of a super capacitor.

## Reference

1. Li G. Shi D.H, Zhu H.L, Yan H, Ng S.W. (2007). Transition metal complexes (*M* = Cu, Ni and Mn) of Schiff-base ligands: Syntheses, crystal structures and inhibitory bioactivities against urease and xanthine oxidase. Inorg. Chim. Acta 2007, 360, 2881–2889.
2. Johns C.A, Golzar-Hossain G.M, Abdul-Malik K.M, Zahir-Haider S, Rowzatur-Romman. (2001).U.K.Structural studies of Ni(II), Zn(II) and Cd(II) complexes with saccharinate and 2,2'-bipyridine ligands. Polyhedron, 20, 721–726.
3. Tomczyk P, Mordarski G, Oblakowski J. (1993). J. Electroanal. Chem.,353, 177.
4. Makkus R. C, Hemmes K, Wir J. H. W. D. (1994).J. Electrochem. Soc.141, 3429.
5. Hotovy I, Huran J, Spiess L, Romanus H, Buc D, Kosiba R. (2006).NiO-based nanostructured thin films with Pt surface modification for gas detection. Thin Solid Films, vol. 515, no.2, pp. 658–661.
6. Thota,Kumar J.(2007). Sol-gel synthesis and anomalous magnetic behaviour of NiO nanoparticles. Journal of Physics and Chemistry of Solids, vol. 68, no. 10, pp. 1951–1964, [8].
7. Fujii E, Tomozawa A,Torii H. Takayama R .(1996). Jpn. J. Appl.Phys.35, L328.
8. Jayalakshmi M, Balasubramanian K. (2008) . Int. J. Electrochem. Sci. 3 1196.
9. Schmidt, G.(2004) Nanoparticles: From Theory to Application; VCH: Weinheim, Germany.
10. Granqvis C.G.(1995).(Ed.), Handbook of Inorganic Electrochromic Materials, Elsevier,Amsterdam.
11. Zhang F.B , Zhou Y.K , Li H.L. (2004) Nanocrystalline NiO as an electrode material for electrochemical capacitor. Mater. Chem. Phys, 83, 260–264.
12. Leevin D, Ying J.Y.( 1997) Oxidative dehydrogenation of propane by non-stoichiometric nickel molybdates. Stud. Surf. Sci. Catal, 110, 367–373.
13. Lunkenheimer P, Loidl A.(1991).Phys. Rev. B: Condens. Matter,44, 5927.
14. Sheela B, Gomathi H, Prabhakara Rao G. (1995) J. Electroanal.Chem.,394, 267.

15. Hosny.N.M.(2011).Synthesis,characterization and optical band gap of NiO nanoparticles derived from anthranilic acid precursors via a thermal decomposition route, Polyhedron, 30 470-476.
16. Surca A, Orel B, Pihlar B, Bukovec P . (1996) .J. Electroanal. Chem. 408 83.
17. Chen R.-Y, Zhou K.-G.(2006).Preparation of ultrafine nickelpowder by wet chemical process, Transactions of Nonferrous Metals Society of China, vol. 16, no. 5, pp. 1223–1227.
18. Cullity B. (1987). Elements of X-ray Diffraction, Addision-Wesley, Reading, p. 294.
19. Mohammadijoo M, Naderi Khorshidi Z, Sadrnezhaad S.K, Mazinani V.Synthesis and characterization of nickel oxide nanoparticle with wide band gap energy prepared via thermochemical processing.I.J Nanoscience and Nanotechnology.
20. Subramanian Saravanakumar, Ramachandran Saravanan,Subramanian Sasikumar (2014). Effect of sintering temperature on the magnetic properties and charge density distribution of nano-NiO. Chemical Papers 68 (6) 788–797
21. Prabhu Y.T,Venkateswara K.R. Sesha V.S.K ,Siva Kumari B.(2013). X-ray analysis of Fe doped ZnO nanoparticles by Williamson-Hall and size-strain methods. Int. J. Engg. Adv. Tech.2 (4), P. 268.
22. Mote V.D, Purushotham Y, Dole B.N. (2012). Williamson-Hall analysis in estimation of lattice strain in Nanometer-sized ZnO particles. J. Theor Appl. Phys. 6:1-8.
23. Williamson G.K. Hall W. H (1953).X-ray line broadening from led Al and W.Act Metall.1,P. 22.
24. Fernandez G.M, Martnez-Arias A, Hanson J.C ,Rodrguez J.A. (2004).Nanostructured oxides in chemistry: Characterization and properties.Chem.Rev.104, P.4063.
25. Ahmad M.I, Bhattacharya S.S. (2009). Appl. Phys. Lett.95191906.
26. Li G, Boerio-Goates J, Wood field B.F, Li L .(2004). Appl. Phys. Lett. 85 2059.
27. Manoranjan Ghosh, Debjani Karmakar, Gadkari S.C, Gupta S.K , Basu S.Effect of size and aspect ratio on structural parameters and evidence of shape transition in zinc oxide nanostructures:BARC, Mumbai, India
28. Thirugnanasambandan ,Theivasanthi ,Marimuthu Alagar,Titanium dioxide (TiO2) Nanoparticles - XRD Analyses – An Insight
29. Jiji A, Joseph N, Donald R.B, Daniel M, Amit S, You Qiang. (2006). Size-Dependent Specific Surface Area of Nanoporous Film Assembled by Core-Shell Iron Nanoclusters. J.Nanomater. (54961): 1-4.
30. Jo-Yong Park, Yun-Jo Lee, Ki-Won Jun, Jin-Ook Baeg ,Dae Jae Yim ( 2006) .Chemical Synthesis and Characterization of Highly Oil Dispersed MgO Nanoparticles. J.Ind.and Eng Chem.12(6), pp.882-887.
31. Zhang J, Xiao X, Nan J. (2010) .Hydrothermal–hydrolysis synthesis and photocatalytic properties of nano $TiO_2$ with an adjustable crystalline size. J.Hazardous Mat. 176: 617-622.
32. Bashar Issa, Ihab Obaidat M, Borhan Albiss A, Yousef Haik.(2013).Magnetic Nanoparticles: Surface Effects and Properties Related to Biomedicine Applications. Int J Mol Sci. 14(11): 1266 –21305.
33. Noack V, Eychmuller A.(2002) Chem.Mater,14, 1411–1417.
34. Kanthimathi M, Dhathathreyan A, Nair B.V. (2004).Nanosized nickel oxide using bovine serum albumin as template, Mater. Lett. 58 2914–2917.
35. Lange F.F (1989), Powder processing science and technology for increased reliability, J.Am Ceram Soc, 72 3-1.
36. Gorschluter ,Merz H.(1994) Phys. Rev. B, 49, 17293.
37. Fromme B, Moller M , Anschutz Th, Bethke C ,Kisker E (1996). Phys. Rev. Lett. 77 1548.
38. Tsuboi T, Kleeman W. (1994). J. Phys. Condensed Matter 6 8625.
39. Anandan K, Rajendran V. (2011).Morphological and size effects of nio nanoparticles via solvothermal process and their optical properties. Mater. Sci. Semicond. Process.
40. Chizallet C, Costentin G, Lauron-Pernot H, Che M, Bonhomme C.(2007). Study of the Structure of OH Groups on MgO by 1d and 2d 1H MAS NMR Combined with DFT Cluster Calculations, J. Physical Chemistry *C*, Vol.111, No. 49, pp.18279-18287.
41. Larichev Y.V, Moroz B.L, Zaikovskii V.I, Yunusov S.M, Kalyuzhnaya E.S. (2007). XPS and TEM Studies on the Role of the Sup- port and Alkali Promoter in Ru/MgO and Ru-Cs/MgO Catalysts for Ammonia Synthesis. J.Physical Chemistry C, Vol. 111, No. 26,pp. 9427-9436.
42. Dubal. D. P. Jagadale A. D ,Patil. S. V, Lokhande C. D (2012) Materials Research Bulletin 47 1239 .
43. Condoba-torressi S.I, Hugot-Legoff A,Joiret S.J (1991).J.Electrochem.Soc .1381554.
44. Chigane M, Iskikawa M.(1994).J.Electrochem.Soc 1413439.
45. Tong X, Qin Y, Guo X, Moutanabbir O, Ao X. (2012).Enhanced catalytic activity for methanol electro-oxidation of uniformly dispersed nickel oxide nanoparticles - carbon nanotube hybrid materials. 8(22):3390–3395.
46. Rahim A, Abdel Hameed R, Khalil M (2004). Nickel as a catalyst for the electro-oxidation of methanol in alkaline medium. J .Power Sources 134(2):160–169.
47. Lang J.W, Kong L.B, Wu W.J, Luo Y. C, Kang L. (2008) Chem. Commun, 35 4213.
48. Srinivasan V, Weidner J. W (1997). J. Electrochem. Soc, 144 L210.
49. Li H, Wang J, Chu Q, Wang Z, Zhang F, Wang S .(2009). J. Power Sources, 190, 578.
50. Nam K.W, Lee C.W, Yang X.Q, Cho B.W,Yoon W.S,.(2009.J. Power Sources . 188, 323.
51. Bard A.J, Faulkner L. R, (2001).Electrochemical Methods: Fundamentals and Applications, John Wiley & Sons, Hoboken, NJ, USA.
52. Eisele S, Schwarz M, Speiser B, Tittel C. [2006].Electrochim. Acta; 51: 5304.